Chemistry of Metals and Alloys

Chem. Met. Alloys 7 (2014) 139-148
Ivan Franko National University of Lviv
www.chemetal-journal.org

$Ag_3Ge_2S_5Br$: Synthesis, structure and ionic conductivity

Mykola MOROZ[1]*, Pavlo DEMCHENKO[2], Vitaliy ROMAKA[3], Roman SERKIZ[4], Lev AKSELRUD[2], Roman GLADYSHEVSKII[2], Oleksiy MYKOLAYCHUK[5]

[1] *Department of Chemistry and Physics, National University of Water Management and Nature Resources Use, Soborna St. 11, UA-33028 Rivne, Ukraine*
[2] *Department of Inorganic Chemistry, Ivan Franko National University of Lviv, Kyryla i Mefodiya St. 6, UA-79005 Lviv, Ukraine*
[3] *Department of Materials Engineering and Applied Physics, Lviv Polytechnic National University, Ustyyanovycha St. 5, UA-79013 Lviv, Ukraine*
[4] *Scientific-Technical and Educational Center of Low Temperature Studies, Ivan Franko National University of Lviv, Drahomanova St. 50, UA-79005 Lviv, Ukraine*
[5] *Department for Metal Physics, Ivan Franko National University of Lviv, Kyryla i Mefodiya St. 8, UA-79005 Lviv, Ukraine*
** Corresponding author. Tel: +380 362 235084; e-mail: riv018@i.ua*

Received December 8, 2013; accepted December 24, 2014; available on-line September 1, 2015

A new compound, $Ag_3Ge_2S_5Br$, was found on the intersection of the Ag_3SBr–GeS_2 and $Ag_2Ge_2S_5$–AgBr polythermal cross-sections of the Ag_2S–GeS_2–AgBr system. The peritectic process $L + GeS_2 \leftrightarrow Ag_3Ge_2S_5Br$ takes place at T = 727 K. The crystal structure of $Ag_3Ge_2S_5Br$ was solved and refined using X-ray powder diffraction data: own structure type, space group $P2_13 - b^2a^5$, Pearson symbol $cP44$, Z = 4, a = 10.16702(7) Å, R_I = 0.0395, χ^2 = 3.19. $Ag_3Ge_2S_5Br$ was also obtained in the glassy state. The charge and mass transfer of the crystalline and glassy phases was investigated by the *dc* probe method between 250 and 495 K. The samples are purely ionic (Ag^+, Br^-) conductors. The influence of lining of the transport channels by the halogens (Br^-, I^-) on the conductivity of crystalline ($Ag_3Ge_2S_5Br$ + 10 wt.% GeS_2) and glassy ($Ag_3Ge_2S_5Br$) samples was studied. Electronic structure calculations (FP-LAPW method) support the experimental results.

Ag–Ge–S–Br / Phase formation / Crystal structure / Electrical conductivity / Superionics / DFT calculations

1. Introduction

The formation of two quaternary compounds, $Ag_6GeS_4Br_2$ (**I**) [1,2] and Ag_3GeS_3Br (**II**) [3], has been established in the Ag–Ge–S–Br system. Their compositions lie in the Ag_2S–GeS_2–AgBr plane of the Gibbs concentration tetrahedron. The positions of compounds in this plane are determined by the points of intersection of two-phase equilibria lines. For **I** these lines are Ag_4GeS_4–AgBr and Ag_2GeS_3–GeS_2, and for **II** Ag_3SBr–GeS_2 and Ag_2GeS_3–AgBr. **I** forms from the melt at T = 676 K following the peritectic reaction $L + Ag_8GeS_6 \rightarrow Ag_6GeS_4Br_2$, while for **II** the process $L + Ag_2GeS_3 \rightarrow Ag_3GeS_3Br$ takes place at T = 718 K. A condition for the synthesis of quaternary compounds in closed containers is that the vapor pressure $p > 10^5$ Pa. With the decline of the gas-phase pressure, decomposition is observed, in spite of condensation of the constituents on the container walls. The sample containing **I** was quenched from T = 670 K as a single phase. **II** has not been obtained as a crystalline single phase, but a melt containing **II** was quenched as a transparent glass of red color. Charge and mass transfer in the crystalline phase **I** and the glassy phase **II** is provided by silver cations and halogen anions. The parameters of conductivity σ and ΔE allow assigning both **I** and **II** to the class of superionic materials. The formation of the Ag_7GeS_5Br compound [4,5] was not confirmed in [2]. The T–x space of the Ag_2S–GeS_2–AgBr plane in the Ag_2GeS_3–GeS_2–AgBr region remains unexplored. The "relay mechanism movement" of drift motion of Ag^+ with the assistance of I^- in a glass of the Ag_2GeS_3–AgI system is described in [6]. The dynamics of Li^+ movement in halide-substituted superionic argyrodites was investigated in [7].

The aim of this work was to study the equilibrium crystalline and glassy states of samples formed near the point of intersection of the $Ag_2Ge_2S_5$–AgBr and Ag_3SBr–GeS_2 lines, to solve and refine the crystal

structure of the new phase $Ag_3Ge_2S_5Br$ (**III**), and to determine the parameters and mechanism of electrical conductivity of the samples.

2. Experimental

2.1. Sample preparation and characterization

The *T*–*x* space of the Ag_2S–GeS_2–AgBr plane near the point of intersection of the $Ag_2Ge_2S_5$–AgBr and Ag_3SBr–GeS_2 lines was studied using differential thermal analysis (DTA), microstructure analysis (MSA), scanning electron microscopy (SEM), energy-dispersive X-ray spectroscopy (EDX), and X-ray powder diffraction (XRPD).

Samples for the investigation were prepared from thoroughly mixed powders of Ag_2GeS_3, AgBr, Ag_3SBr, and GeS_2 of semiconductor grade. An additional 10 wt.% GeS_2 was added to the stoichiometric amount for the crystalline samples, to avoid dissociation of $Ag_3Ge_2S_5Br$. The solid-state phase synthesis was carried out at $T \approx 710$ K for 50-80 h with 3-5 intermediate grindings, in quartz ampoules evacuated down to a residual pressure of ~1 Pa. The samples were cooled down to $T = 300$ K at the rate of ~15 K/min. After grinding to a particle size of 2-5 μm, the material, of dark red color, was used for DTA, XRPD and $\sigma(T)$ measurements.

DTA measurements were performed on a VDTA-1069 device; the weight of the samples was 0.5-1 g, the heating (cooling) rate 6-8 K/min, and the temperature range 295-930 K. The temperatures were determined with an accuracy better than ±5 K. Glassy samples were obtained by quenching melts of a total weight of ~5 g from $T \approx 1150$ K into ice-water. The density of the glass was determined by hydrostatic weighing. The temperatures of crystallization and glass formation were determined from DTA curves.

MSA was performed by visual observation based on the differences in color of the phases in an optical microscope PMT-3. The composition of the samples was examined by SEM using a REMMA-102-02 scanning electron microscope. EDX was carried out exactly on the grains of the quaternary phase, by using an energy-dispersive X-ray analyzer with the pure elements as standards for Ag and Ge, ZnS for S, and KBr for Br (the acceleration voltage was 20 kV; *K*- and *L*-lines were used).

XRPD data were collected in the transmission mode on a STOE STADI P diffractometer at $T = 297.0(1)$ K. Preliminary data processing and X-ray phase analysis were performed using the STOE WinXPOW [8] and PowderCell [9] program packages. The crystal structure of the new compound $Ag_3Ge_2S_5Br$ was solved by direct methods, using WinCSD-2010 [10], and was refined by the Rietveld method [11] with the program FullProf.2k (version 5.20) [12] from the WinPLOTR package [13], applying a pseudo-Voigt profile function and isotropic approximation for the atomic displacement parameters. An absorption correction was considered by measuring the absorption factor for a sample transmission foil according to [8] and applied during the Rietveld refinement, according to the type "Transmission geometry (STOE)" [12]. Quantitative phase analysis was performed during the Rietveld refinement according to [14]. The crystallographic data were standardized with the program STRUCTURE TIDY [15], and the program DIAMOND [16] was used for structural visualization.

2.2. Conductivity measurements

The electrical conductivity of glassy and crystalline samples was measured in the temperature range 250-495 K (±2 K) by the *dc* probe method in argon at a pressure of ~10^5 Pa. Three types of electrochemical cell (ECC) were used in the measurements: Ag|sample|Ag (*a*), Ag|sample|Ag_3SBr|Ag (*b*), and Ag|sample|Ag_3SI|Ag (*c*) with Ag|(Ag+Ag_3SBr)|sample probes, where (Ag+Ag_3SBr) means a mechanical mixture of finely dispersed silver with silver sulfide-bromide. Such a mixture provides ohmic contact with the sample. The intermediate Ag_3SBr and Ag_3SI layers, pressed into the ECC (*b*) and (*c*), are expected to re-inject halogen anions into the sample and block the electronic component of the conductivity [17,18]. The cells had the form of Teflon bars measuring 10×10×45 mm, with a hole of 2 mm diameter along their length. The powdered components of the cells were pressed into the hole to a density of $\rho = (0.93\pm0.02)\rho_0$, where ρ_0 is the crystallographic density of the compound or cast glassy sample. The lateral side of the cells had three 0.8 mm-diameter holes in its central part at 5 and 10 mm from each other. These holes were filled with the probe electrode material under mechanical pressure. The resistance of the probe contacts was determined by extrapolating the resistance between the probes to zero probe separation. The length of the samples in the ECC was 33-35 mm, the thickness of the Ag_3SBr and Ag_3SI layers was ~3 mm, and the height of the probe contacts was ~2 mm. The silver layer in the current electrodes was ~1 mm thick. The cells were connected in series to the electrical circuit. The electrode on the left hand-side in the circuit scheme had the highest potential. The current through the circuit was $5\cdot10^{-8}$ A, and the input resistance of the voltmeter was $>10^{10}$ Ω. The conductivity σ of the samples was calculated using Ohm's law for the non-uniform portion of the circuit.

2.3. Electronic structure calculations

We used an all-electron full-potential linearized augmented-plane wave (FP-LAPW) method, which performs DFT calculations using the Generalized Gradient Approximation with wave functions as a basis [19]. The Kohn-Sham equation and energy functional were evaluated consistently using the FP-LAPW method. For this method, the space is divided into interstitial and non-overlapping muffin tin

spheres centered on the atomic sites. The basis function inside each atomic sphere is a linear expansion of the radial solution of a spherically potential multiplied by spherical harmonics. In the interstitial region, the wave function is taken as an expansion of plane waves and no shape approximation for the potential is introduced in this region. The core electrons are described by atomic wave functions, which are solved relativistically using the current spherical part; the valence electrons were also treated relativistically in our case. The FP-LAPW calculations were performed with the crystallographic parameters obtained from XRPD.

3. Results and discussion

*3.1. Peculiarities of the formation of $Ag_3Ge_2S_5Br$ (**III**)*

In general, quaternary compounds form if intermediate compounds exist in the quasi-binary systems that delimit the quasi-ternary concentration space. Physical-chemical criteria for the formation of ternary and multicomponent tetrahedral phases have been formulated in [20,21]. The composition $Ag_3Ge_2S_5Br$ is determined by the point of intersection of the $Ag_2Ge_2S_5$–AgBr and Ag_3SBr–GeS_2 lines of the Ag_2S–GeS_2–AgBr concentration plane. It has been established that $Ag_2Ge_2S_5$ cannot be obtained by solid-state synthesis from a vacuum-processed equimolar mixture of Ag_2GeS_3 and GeS_2 [22]. $Ag_2Ge_2S_5$ is a thermally unstable atomic association and forms only at $p >> 10^5$ Pa [23]. In the *p–T–x* space for Ag_2S–GeS_2–AgBr, $Ag_3Ge_2S_5Br$ forms at $T = 727$ K through a peritectic reaction of melt with GeS_2. Sufficient pressure of the gas phase above the melt is a necessary condition for the peritectic process. Single-phase $Ag_3Ge_2S_5Br$ could not be obtained by vacuum ampoule solid-state synthesis from Ag_2GeS_3 +GeS_2 + AgBr or Ag_3SBr + 2GeS_2 mixtures at $T = 710$ K for 12 h. Together with the $Ag_3Ge_2S_5Br$ phase, a structurally-disordered and X-ray amorphous material of greenish-grey color (~30 vol.%) was detected by XRPD and MSA. Regrinding and increasing the synthesis time up to 160 h did not promote the crystallization process, in spite of the low pressure of the gas phase above the sample. Molecular GeS_2 is characterized by a significant pressure even at relatively low temperatures. Adding an excess of GeS_2 (≥ 10 wt.%) to the stoichiometric amounts of the starting components significantly reduced the time required to reach the equilibrium state, which took the form of a two-phase mixture of the quaternary phase and GeS_2. With decreasing temperature ($T < 650$ K), and hence reduced gas-phase pressure in the closed container, the mixture slowly decomposed. However, quenched crystalline $Ag_3Ge_2S_5Br$ + 10 wt.% GeS_2 (**III**-GeS_2) and glassy $Ag_3Ge_2S_5Br$ (**III**(g)) were found to be stable during repeated thermal cycling (250-500 K) in an inert argon atmosphere ($p \geq 10^5$ Pa).

Fig. 1a shows a typical crystalline specimen of $Ag_3Ge_2S_5Br$. Due to the difficulty of the synthesis, pure single-phase samples were not obtained. SEM and XRPD patterns showed small amounts of dielectric GeS_2 between the grains of the quaternary phase. The primary particles of $Ag_3Ge_2S_5Br$ displayed a size in the range of 2-5 μm and cubic shape (Fig. 1b). The EDX analysis performed on the grains of the quaternary phase (Fig. 1c) showed the following composition (in at.%, with an accuracy of 4 %, measured/calculated) Ag: 24.4/27.27, Ge: 19.6/18.18, S: 44.2/45.46, Br: 11.8/9.09.

*3.2. Crystal structure of **III***

Once the crystal structure was solved and an appropriate structural model for the quaternary compound had been found, a structural refinement was made using XRPD data for the $Ag_3Ge_2S_5Br$ sample containing also monoclinic GeS_2 (space group *Pc*) [24], stable at ambient conditions. X-ray experimental and crystallographic data for $Ag_3Ge_2S_5Br$ are summarized in Table 1, while the final atomic and displacement parameters are listed in

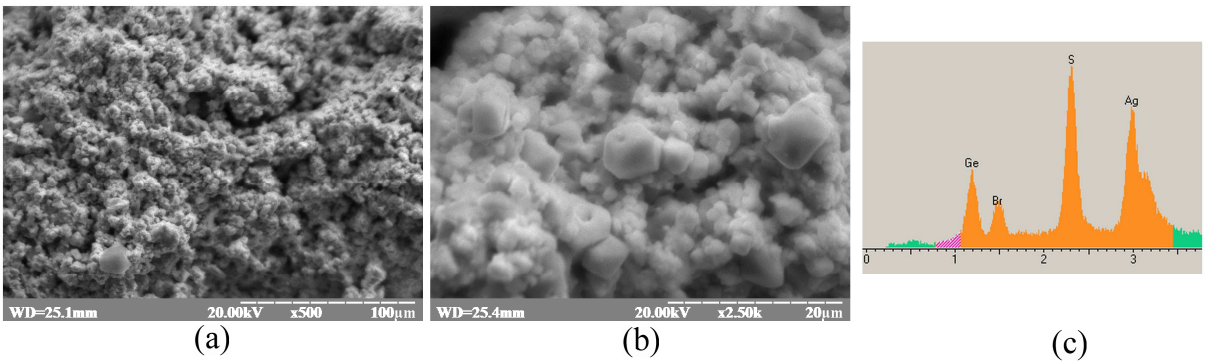

Fig. 1 SEM pictures of the crystalline $Ag_3Ge_2S_5Br$ sample **III**-GeS_2: (a) general view (×500) showing the inclusion of the impurity phase GeS_2 as fine grains of grey color; (b) detailed view (×2500) of $Ag_3Ge_2S_5Br$ particles displaying cubic shape; (c) part of the EDX spectrum showing Ge *L*, Br *L*, S *K* and Ag *L*-lines.

Table 2. A comparison of the experimental and calculated powder patterns is presented in Fig. 2. Interatomic distances and atomic environments are given in Table 3. The shortest interatomic distance in the structure is Ge2–S3 (2.079(4) Å), however, it can be in agreement with data given in [25] ("smallest 5 %" for Ge^{4+}–S^{2-} is 2.084 Å). The presence of strong bonding in this case is indirectly confirmed by the low value of the displacement parameter for S3.

The total electron balance for $Ag_3Ge_2S_5Br$ is in good agreement with the formal charges of the ions: $(Ag^{1+})_3(Ge^{4+})_2(S^{2-})_5(Br^{1-})_1$. Calculating the parameters proposed by Parthé to test for the possible formation of tetrahedral structures [21,26], *i.e.* the valence-electron concentration per atom (VEC) and the valence-electron concentration per anion (VEC_A), the following values are obtained: VEC = 4.364, VEC_A = 8. The latter number indicates that $Ag_3Ge_2S_5Br$ is a normal valence (ionic-covalent) compound and the former that it may adopt a defect tetrahedral structure with N_{NBO} = 0.364 (4/11) (where N_{NBO} is the average number of non-bonding orbitals or lone-electron pairs per atom). This assumption was confirmed by the structural refinement and the crystal

Table 1 Experimental details and crystallographic data for $Ag_3Ge_2S_5Br$.

Formula / name	$Ag_3Ge_2S_5Br$ / trisilver digermanium pentasulfide bromide
Space group – Wyckoff sequence / Pearson symbol	$P2_13$ (No. 198) – b^2a^5 / $cP44$
Mass per formula unit / Z	709.00 / 4
Lattice parameter a (Å)	10.16702(7)
Cell volume V (Å^3)	1050.946(13)
F(000) (electrons)	1280
Calculated density D_x (g/cm^3)	4.481
Absorption coefficient μ (Cu $K\alpha$) (mm^{-1})	63.81
Specimen shape / particle morphology / color	Flat sheet (8×8×0.1 mm) / loose powder, grain size < 0.005 mm / dark red
Data collection temperature T (K)	297.0(1)
Diffractometer	STOE STADI P (transmission mode)
Radiation, wavelength λ (Å)	Cu $K\alpha_1$, 1.540598
Angular range for data collection / increment (°2θ)	6.000 ≤ 2θ ≤ 124.410 / 0.015
Linear PSD step (°2θ) / time (sec/step)	0.480 / 675
Number of measured reflections	341
Number of refined parameters	27
Half width parameters η_0, U, V, W	0.369(4), 0.0192(9), –0.0081(8), 0.0105(2)
Asymmetry parameters As1, As2	0.075(2), 0.0172(6)
Reliability factors:	
$R_I = \Sigma\|I_{obs}–I_{calc}\| / \Sigma\|I_{obs}\|$	0.0395
$R_F = \Sigma\|F_{obs}–F_{calc}\| / \Sigma\|F_{obs}\|$	0.0433
$R_p = \Sigma\|y_i – y_{c,i}\| / \Sigma y_i$	0.0418
$R_{wp} = [\Sigma w_i \|y_i – y_{c,i}\|^2 / \Sigma w_i y_i^2]^{1/2}$	0.0561
$R_{exp} = [n–p / \Sigma w_i y_i^2]^{1/2}$	0.0314
$\chi^2 = \{R_{wp}/R_{exp}\}^2$	3.19
Content of $Ag_3Ge_2S_5Br$ / GeS_2 (wt.%)	89.4(3) / 10.6(1)

Table 2 Fractional atomic coordinates and isotropic displacement parameters for $Ag_3Ge_2S_5Br$.

Site	Wyckoff position	x	y	z	B_{iso} (Å^2)
Ag	12*b*	0.18030(13)	0.53414(13)	0.33866(12)	4.89(4)
Ge1	4*a*	0.14805(14)	0.14805(14)	0.14805(14)	0.85(6)
Ge2	4*a*	0.61055(18)	0.61055(18)	0.61055(18)	1.31(7)
S1	12*b*	0.1092(4)	0.3617(4)	0.1303(4)	1.64(6)
S2	4*a*	0.0119(5)	0.0119(5)	0.0119(5)	2.77(17)
S3	4*a*	0.7286(3)	0.7286(3)	0.7286(3)	0.42(15)
Br	4*a*	0.38258(19)	0.38258(19)	0.38258(19)	2.24(7)

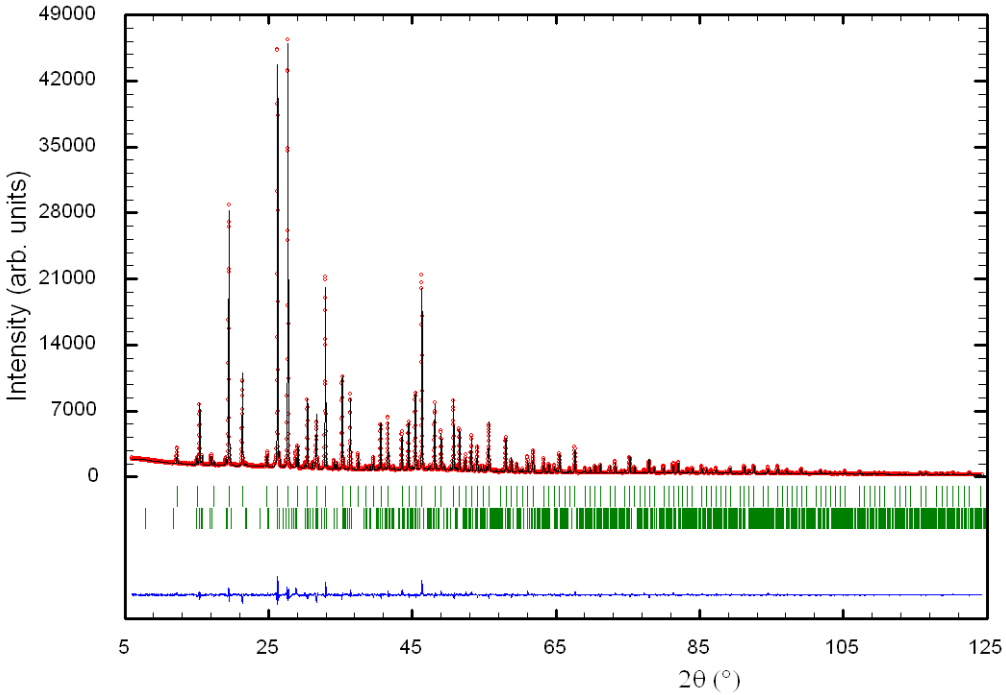

Fig. 2 Observed and calculated X-ray powder profiles for the crystalline $Ag_3Ge_2S_5Br$ sample **III**-GeS_2. Experimental data (circles) and calculated profile (solid line through the circles) are presented together with the calculated Bragg positions (vertical ticks) and difference curve (bottom solid line). Top ticks: $Ag_3Ge_2S_5Br$ (89.4(3) wt.%); bottom ticks: GeS_2 (10.6(1) wt.%).

Table 3 Interatomic distances (δ), coordination numbers (CN) and coordination polyhedra for $Ag_3Ge_2S_5Br$ with crystal chemical formula $^{3}_{\infty}Ag_3^{[4t]}Ge_2^{[4t]}\underline{S}_3^{[3n]}S^{[4y]}S^{[4t]}\underline{Br}^{[3n]}$.

Bond	δ(Å)	CN	Coordination polyhedron
Ag – S2	2.486(5)	4	tetrahedron [4t]
– S3	2.555(3)		**Ag**[S_3Br]
– Br	2.608(2)		
– S1	2.843(4)		
Ge1 – 3S1	2.215(4)	4	tetrahedron [4t]
– S2	2.398(5)		**Ge1**[S_4]
Ge2 – S3	2.079(4)	4	tetrahedron [4t]
– 3S1	2.261(4)		**Ge2**[S_4]
S1 – Ge1	2.215(4)	3	non-coplanar triangle [3n]
– Ge2	2.261(4)		(ψ-tetrahedron [3n])
– Ag	2.843(4)		**S1**[Ge_2Ag]
S2 – Ge1	2.398(5)	4	triangular pyramid [4y]
– 3Ag	2.486(5)		(distorted tetrahedron [4t])
			S2[$GeAg_3$]
S3 – Ge2	2.079(4)	4	tetrahedron [4t]
– 3Ag	2.555(3)		**S3**[$GeAg_3$]
Br – 3Ag	2.608(2)	3	non-coplanar triangle [3n]
			(ψ-tetrahedron [3n])
			Br[Ag_3]

chemical formula can be written as $^{3}_{\infty}Ag_3^{[4t]}Ge_2^{[4t]}\underline{S}_3^{[3n]}S^{[4y]}S^{[4t]}\underline{Br}^{[3n]}$ (see Table 3), where the bars under S and Br indicate lone-electron pairs. Since S1 and Br have defect tetrahedral coordination (non-coplanar triangles), four lone-electron pairs in total can be assigned to these anions. Slightly distorted Ge[S_4] and Ag[S_3Br] tetrahedra share all corners to form a 3D-framework (Fig. 3a).

The anionic framework of the structure consists of four empty distorted tetrahedra [$S1_3Br$], four single S2 and four single S3 anions in the unit cell. Expanding the unit cell range to $-0.012 < (x, y, z) < 1.012$, makes it easier to see the approximate fcc stacking of the S2 anions. The anionic framework shown in Fig. 3b is similar to the arrangement of the atoms in the cubic Laves phase $MgCu_2$, which is also true for the structure of argyrodite [27,28]. The general formula of the argyrodite family $(A^{m+})_{(12-n-y)/m}B^{n+}(X^{2-})_{6-y}(Z^{-})_y$ (where A = Ag^+, Cu^+, *etc.*; B = Ge^{4+}, P^{5+}, *etc.*; X = chalcogen; Z = halogen) does not include the composition $Ag_3Ge_2S_5Br$. But considering the constituent elements and some common crystal-chemical features (space group, cell parameter, tetrahedrally close-packed anionic framework), this compound may be referred to as a *quasi*-argyrodite. While for $Ag_6GeS_4Br_2$ (and for $Ag_6GeS_4Cl_2$), it was stated that "*... new phases with the wanted composition but not with the expected crystal structure were formed surprisingly*" [1], for $Ag_3Ge_2S_5Br$ one may talk about "a new phase with unwanted composition, but with the expected (argyrodite-like) crystal structure".

In the structure of $Ag_3Ge_2S_5Br$, the S and Br anions form a distorted $MgCu_2$-like substructure, providing 136 tetrahedral cation holes per unit cell, 20 of which are fully occupied by 8 Ge and 12 Ag cations. Thus, 116 tetrahedral sites remain unoccupied. According to the classical model for the high ionic conductivity of argyrodites [5,28-30], these unoccupied tetrahedral sites serve as pathways for the jumping migration process of the Cu^+- or Ag^+-cations. High displacement parameters and partial site occupancies are observed for Cu^+ and Ag^+, *i.e.* order-disorder phenomena in the substructure of the *A*-cations facilitate this process.

3.3. Electronic structure of ***III***

Electronic structure calculations showed that the compound is characterized by an energy gap (ΔE = 1.520 eV) between the valence and conduction bands and should consequently exhibit semiconducting properties. The Fermi level (E_F) is situated at the edge of the valence band. The electron density distribution (Fig. 4) shows that the bonds between the Ge and S atoms are very strong, polarized (the electron density is shifted to the S atoms) From the density of electronic states DOS (Fig. 5) it is clear that the *s*- and *p*- states of Ge are hybridized and mainly overlap with *p*-states of S atoms. The *d*-states of the Ag atoms are fully occupied and hence play a non-bonding role, while the valence *s*-shell with one electron mainly overlaps with *p*- and less with *s*-valence shells of the S2 and S3 sulfur atoms. The electron density between sulfur and silver atoms is lower than in the between sulfur and germanium. The bromine atoms show fully occupied *s*- and *p*-states and appear to be weakly bonded to the Ag atoms.

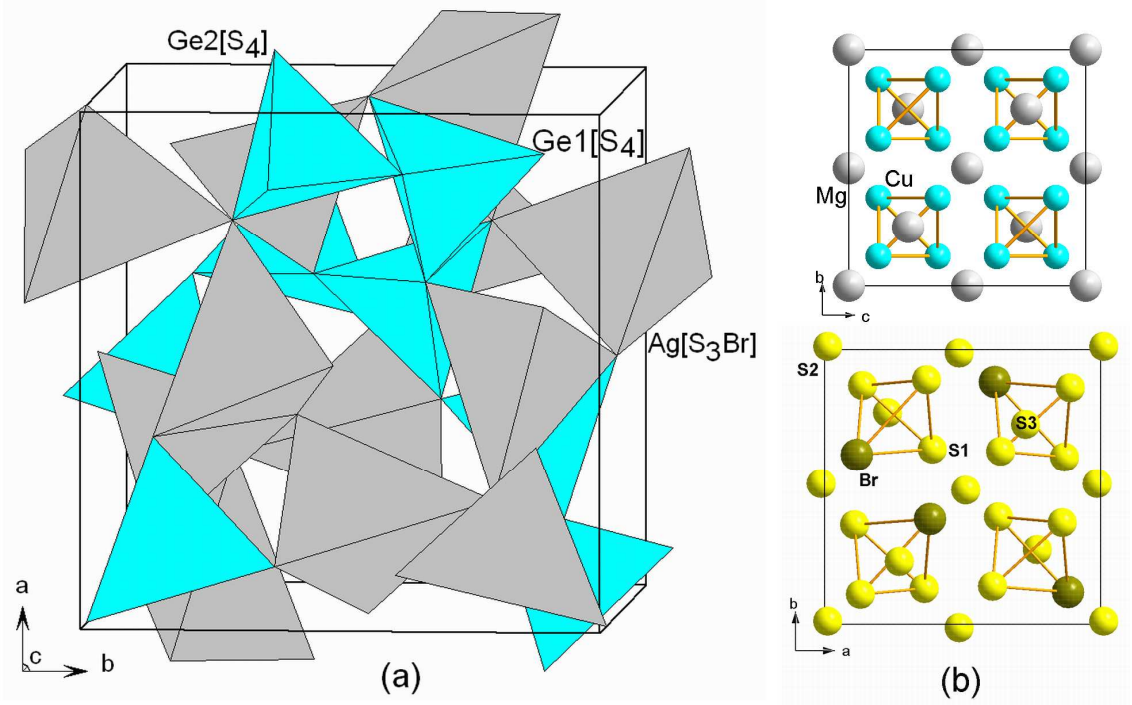

Fig. 3 Crystal structure of $Ag_3Ge_2S_5Br$: (a) 3D-packing of Ge[S_4] and Ag[S_3Br] all-corner-linked tetrahedra (the atoms are not shown for clarity); (b) comparison of the anionic framework in $Ag_3Ge_2S_5Br$ with the structure of $MgCu_2$ (space group *Fd*-3*m*), which is similar to the anionic framework in argyrodites.

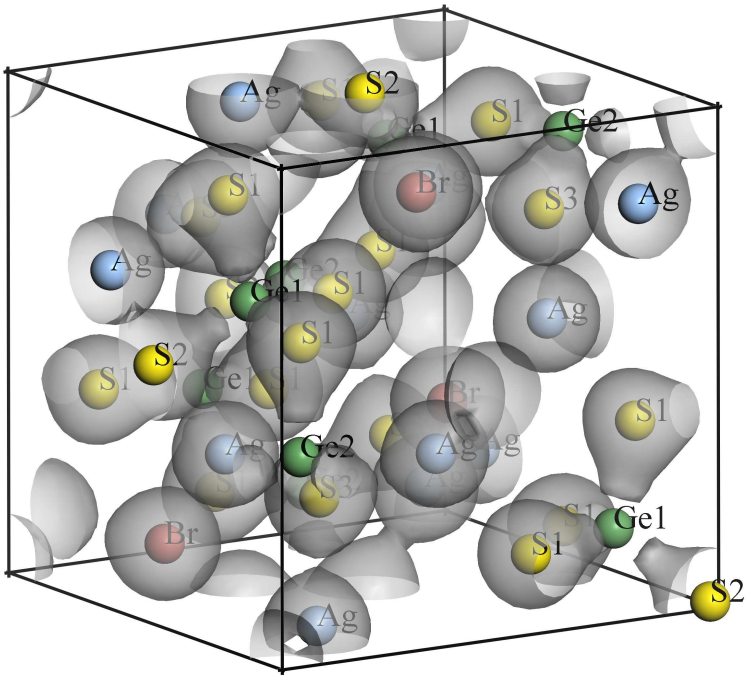

Fig. 4 Isosurface (ρ = 0.4 e/Å^3) of the electron density in one unit cell of $Ag_3Ge_2S_5Br$.

3.4. Electrical conductivity of the crystalline and glassy samples

The temperature dependence of the conductivity of crystalline **III**-GeS_2 and glassy **III**(g) was studied in ECC (*a*)–(*c*). In **III**-GeS_2, GeS_2 serves as dielectric filler. It was found that the same sample at the same temperature showed different values of conductivity (σ) in the three ECC (Fig. 6). Each of the six presented curves contains two straight-line portions. Below 380-400 K $\sigma(T)$ is well described by Arrhenius' law for the case of one type of capture center of charge carriers. At temperatures exceeding 400–420 K the straight-line portions of the curves in semi-logarithmic coordinates are described by Arrhenius' equation with a positive exponent. The reasons for the different values of σ obtained in ECCs of different design are partially analyzed in [2,3,18]. Probe measurements of the distribution of the polarization emf (electromotive force) along the length of pressed crystalline ($Ag_6SnS_4Br_2$, $Ag_6GeS_4Br_2$, Ag_3SBr, Ag_3SI) and glassy (Ag_3GeS_3Br) samples showed heterogeneous distribution of the charge. The excess negative charge concentrates in a narrow field of the sample, near the electrodes (5-7 % of the total length of the sample). In the central part of the sample (more than 65 % of the total length), excess positive charge with a maximum near the middle is formed. The described distribution of the polarization emf along the length of the sample remains infinitely long. This proves that an electronic component of conductivity is absent in these materials. The charge heterogeneity of the samples can be satisfactorily modeled by assimilating the halogen anions to a quasi-liquid in motion. The halogen anions of the pressed material shift towards the electrodes, attracted by the electrostatic forces of the double charge layer formed at the Ag|sample border. The "formula" silver does not display the characteristics of a quasi-liquid in motion, but is an active constituent of the structural units of the crystalline and glassy phases. Electrical and mass transfer is provided by the Ag^+, Br^-, I^--ions injected into the structure of the samples. The electrodes act as a source of drift Ag^+ cations. The appearance of drift halogen anions is associated with electrolysis in the region of the sample with the lowest potential. The σ-values were determined from the concentration of injected charge carriers, and from the value of their drift velocity through the transport migration channels. The transport migration channels of samples with defect structure (*e.g.* unoccupied/occupied tetrahedral sites in the crystal structure, lattice strains, and crystallographic defects), hosting counter-current flows of drifting ions of both signs, should be considered as quantum systems. The interaction of the components of such systems determines the value of the drift velocity of the charge carriers. The "relay mechanism movement" for the drift of Ag^+ with the assistance of I^- in $(AgI)_x(Ag_2S{\cdot}GeS_2)_{1-x}$ glasses was established by ^{109}Ag NMR [6]. It is probable that such a "relay mechanism movement" of charge carriers is takes place in all superionic silver- and halogen-containing solids. The "relay mechanism movement" of charge carriers is characterized by two factors that

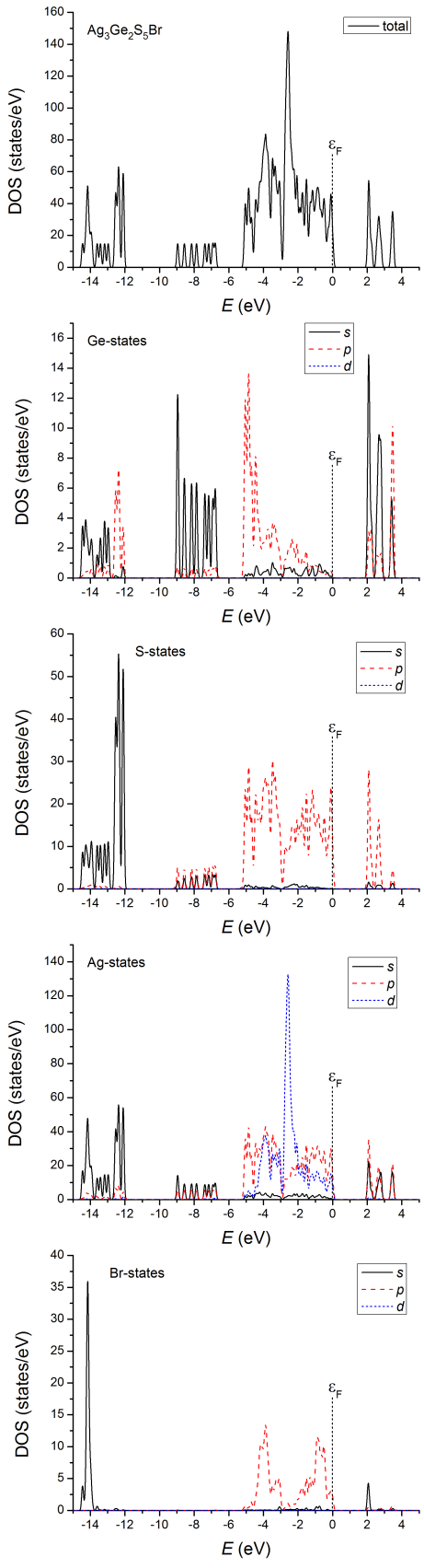

Fig. 5 Distribution of the total and partial density of states for $Ag_3Ge_2S_5Br$.

differently affect the velocity of Ag+. The drift motion of Br – and I – is accompanied by the capture of part of the anions by structural defects in the transport migration channels (lining the channels). The positive charge in the central part of the sample facilitates the process of lining. Augmentation of the linear density of halogens increases the probability of "jumping" of Ag+ from one halogen to another along the direction of the electric field. The result of this process is an increase of the drift velocity of Ag+, and hence of the conductivity of the sample. On the other hand, for some time during the drift motion the charge carriers are in a bound state. The growth of the linear density of bound halogens along the transport channels increases the time of passage per unit path length by the drift Ag+. This factor decreases the drift velocity of the silver ions.

The charge heterogeneity along the sample length in the ECC was characterized both for crystalline **III**-GeS_2 and glassy **III**(g). The curves on Fig. 6 display purely ionic charge transfer involving Ag^+, Br^-, and I^-. The fitting of the conductivity to linear dependence in Arrhenius' coordinates below $T = 420$ K is an indication of a decisive contribution of the drift Ag^+ to σ. The drift Br^- and I^-, captured by defects in the transport channels, manifest themselves as active participants of the "relay mechanism movement" of the silver cations. The difference in σ between the ECCs is due to the different linear density and type of halogen bound to the structure of the transport channels. The electrolysis rate of **III**-GeS_2 and **III**(g) (ECC (*a*)) and of the ternary Ag_3SBr phase (ECC (*b*) and (*c*)) is a factor that limits the linear density of the halogens in the transport channels. Deviation in the temperature dependence of σ from Arrhenius' law is observed at $T > 380$-400 K. At these temperatures, the energy of the thermal vibrations of the atoms is sufficient to break bonds of the lining halogens with the capture centers. The straight-line portions of the curves in the range of 400-495 K represent an exponential decrease of the number of halogens bound to the structure of the transport channels. The result is a decrease of the velocity of drift Ag^+ by the same law. The difference between the absolute values of σ for **III**-GeS_2 and **III**(g) is mainly due to different concentrations of injected silver cations. The reason is in the discrepancy between the total effective cross-section of the transport channels for the crystalline and glassy phases. The significant increase of the specific conductivity of lined glassy **III**(g) (ECC (*b*) and (*c*)), in comparison with non-lined **III**(g) (ECC (*a*)) opens new directions for monitoring the physical properties of solids. The parameters of conductivity and activation energy (Table 4) allow assigning **III**-GeS_2 and **III**(g) to the class of superionic materials. The experimental values of density, temperatures of glass-formation and crystallization of glassy $Ag_3Ge_2S_5Br$ are $\rho = 4.82 \cdot 10^3$ kg/m^3, $T_g = 503$ K, and $T_c = 560$ K, respectively.

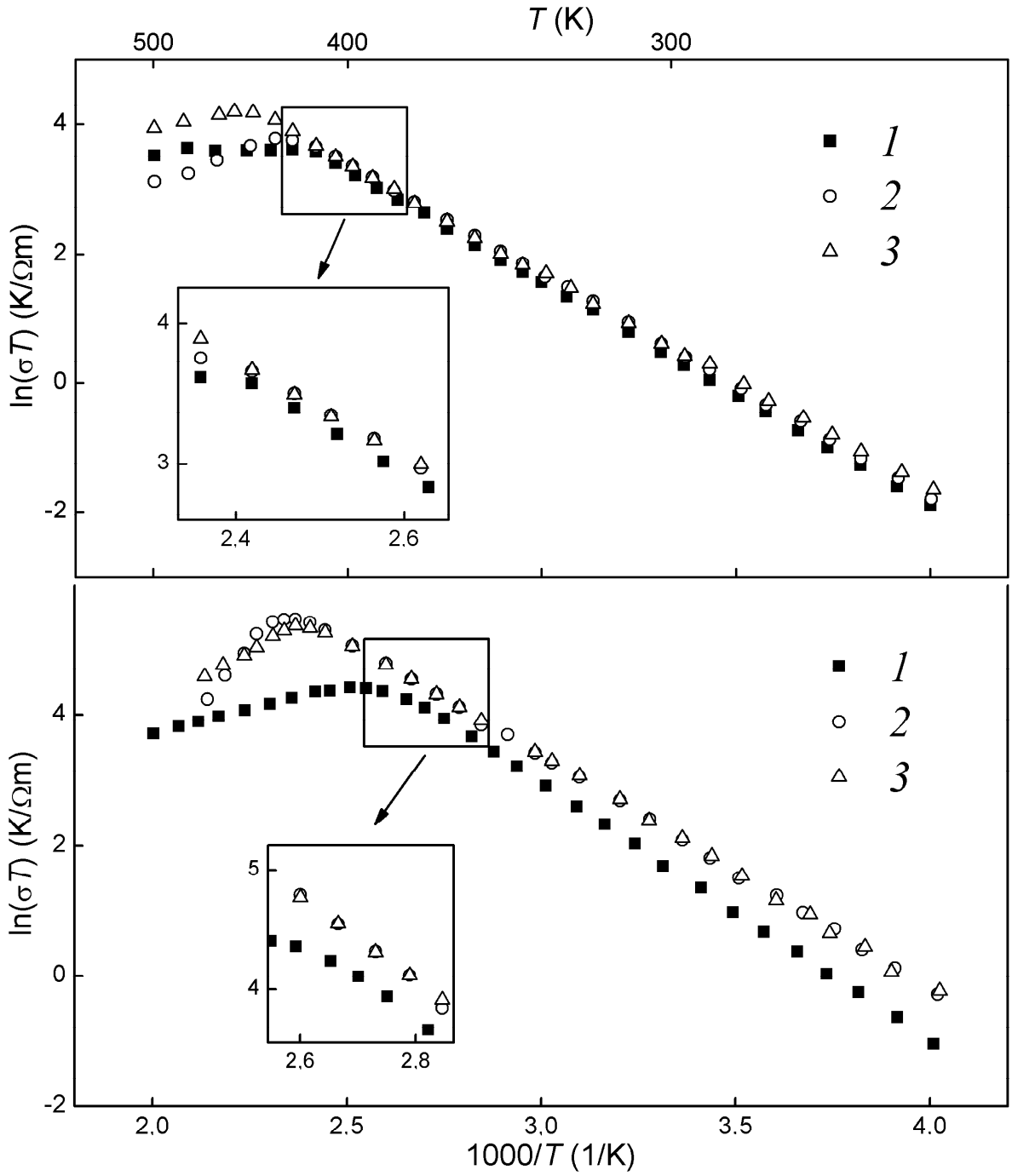

Fig. 6 Arrhenius plots of the conductivity of crystalline $Ag_3Ge_2S_5Br$ + 10 wt.% GeS_2 (top) and glassy $Ag_3Ge_2S_5Br$ (bottom): *1*, *2*, *3* – in ECC (*a*), (*b*) and (*c*), respectively.

4. Conclusions

The existence of a new quaternary compound, $Ag_3Ge_2S_5Br$, has been established in the *p–T–x* space of the quasi-ternary Ag_2S–GeS_2–AgBr system. The crystal structure of $Ag_3Ge_2S_5Br$ (space group $P2_13 - b^2a^5$, Pearson symbol *cP*44, $Z = 4$, $a = 10.16702(7)$ Å, $R_I = 0.0395$, $\chi^2 = 3.19$) belongs to the class of defect tetrahedral structures and can also be referred to as a *quasi*-argyrodite. $Ag_3Ge_2S_5Br$ was also obtained in the glassy state by quenching melts. The halogen anions in the structure of both the crystalline and glassy samples of $Ag_3Ge_2S_5Br$ display the properties of a quasi-liquid in motion, while the silver cations do not show such properties. DFT calculations using the FP-LAPW method support the

experimental results, showing semiconducting properties and strong bonding between the Ge and S atoms. The halogen anions and silver cations injected into the structure provide electrical conductivity. The transfer of drift charge carriers occurs *via* a "relay mechanism movement". The heterogeneous charge distribution along the sample length was characterized for $Ag_3Ge_2S_5Br$ samples with Ag-electrodes. The excess positive charge of the central part of the samples facilitates the capture of drift Br^- or I^- anions by structural defects in the transport migration channels (lining of the channels). The bound halogen anions are active participants of the relay mechanism of the Ag^+ drift motion. The linear density of halogens along the length of the transport channels determines the value of the drift velocity of Ag^+. Crystalline and glassy samples in ECCs of the same design differ by the magnitude of the total effective cross-section of the transport channels, which determines the concentration of drift charge carriers injected into the samples. The samples were found to be purely ionic conductors in the temperature range 250-495 K. At $T = 300$ K the conductivity was $\sigma = 5.08 \cdot 10^{-3}$ $(\Omega \cdot m)^{-1}$ and $\sigma = 1.74 \cdot 10^{-2}$ $(\Omega \cdot m)^{-1}$ for crystalline and glassy $Ag_3Ge_2S_5Br$, respectively.

References

[1] M. Wagener, H.-J. Deiseroth, C. Reiner, *Z. Kristallogr.* 221 (2006) 533.

[2] M.V. Moroz, P.Yu. Demchenko, L.G. Akselrud, O.G. Mykolaychuk, R.E. Gladyshevskii, *Chem. Met. Alloys* 3 (2010) 161.

[3] M. Moroz, P. Demchenko, L. Akselrud, O. Mykolaychuk, R. Gladyshevskii, *Abstr. 17th Int. Conf. Solid Compd. Transition Elem. (SCTE2010)*, Annecy, France, 2010, p. 69.

[4] A. Nagel, K.-J. Range, *Z. Naturforsch. B* 33 (1978) 1461.

[5] M. Laqibi, B. Cros, S. Peytavin, M. Ribes, *Solid State Ionics* 23 (1987) 21.

[6] J. Roos, D. Brinkmann, M. Mali, A. Pradel, M. Ribes, *Solid State Ionics* 28-30 (1988) 710.

[7] H.-J. Deiseroth, S.-T. Kong, H. Eckert, J. Vannahme, C. Reiner, T. Zaiß, M. Schlosser, *Angew. Chem. Int. Ed.* 47 (2008) 755.

[8] *Stoe WinXPOW*, version 3.03, Stoe & Cie GmbH, Darmstadt, Germany, 2010.

[9] W. Kraus, G. Nolze, *PowderCell for Windows*, version 2.4, Federal Institute for Materials Research and Testing, Berlin, March 2000.

[10] L.G. Akselrud, P.Y. Zavalii, Yu.N. Grin, V.K. Pecharski, B. Baumgartner, E. Wölfel, *Mater. Sci. Forum* 133-136 (1993) 335.

[11] R.A. Young (Ed.), *The Rietveld Method*, IUCr Monographs of Crystallography, Vol. 5, Oxford University Press, New York, 1993, 298 p.

[12] J. Rodriguez-Carvajal, *Recent Developments of the Program FULLPROF*, Commission on Powder Diffraction (IUCr), *Newsletter* 26 (2001) 12.

[13] T. Roisnel, J. Rodriguez-Carvajal, *Mater. Sci. Forum* 378-381 (2001) 118.

[14] R.J. Hill, C.J. Howard, *J. Appl. Crystallogr.* 20 (1987) 467.

[15] L.M. Gelato, E. Parthé, *J. Appl. Crystallogr.* 20 (1987) 139.

[16] K. Brandenburg, *DIAMOND. Visual Crystal Structure Information System*, Version 2.1e, Crystal Impact, Bonn, Germany, 2001.

[17] Yu.G. Vlasov, Yu.E. Ermolenko, B.A. Nikolaev, *Elektrokhimiya* 17 (1981) 1448.

[18] O.G. Mykolaychuk, N.V. Moroz, P.Yu. Demchenko, L.G. Akselrud, R.E. Gladyshevskii, *Inorg. Mater.* 46 (2010) 707.

[19] J.P. Perdew, K. Burke, M. Ernzerhof, *Phys. Rev. Lett.* 77 (1996) 3865.

[20] N.A. Goryunova, *Slozhnye Almazopodobnye Poluprovodniki (Complex Diamond-Like Semiconductors)*, Soviet Radio, Moscow, 1968, 268 p.

[21] E. Parthé, *Elements of Inorganic Structural Chemistry*, 2nd Ed., K. Sutter Parthé Publisher, Petit-Lancy, Switzerland, 1996, 170 p.

[22] A.G. Mikolaichuk, N.V. Moroz, *Russ. J. Inorg. Chem.* 55 (2010) 87.

[23] O.P. Kokhan, *Ph.D. Thesis*, Uzhhorod Univ., 1996 (in Ukrainian).

[24] G. Dittmar, H. Schäfer, *Acta Crystallogr. B* 32 (1976) 1188.

[25] G. Bergerhoff, K. Brandenburg, in: *International Tables for Crystallography*, Kluwer Academic Publishers, Dordrecht, 2006, Vol. C, Ch. 9.4, 992 p.

[26] E. Parthé, *Z. Kristallogr.* 119 (1963) 204.

[27] H. Hahn, A. Schulze, L. Sechser, *Naturwissenschaften* 52 (1965) 451.

[28] W.F. Kuhs, R. Nitsche, K. Scheunemann, *Mater. Res. Bull.* 14 (1979) 241.

[29] W.F. Kuhs, R. Nitsche, K. Scheunemann, *Acta Crystallogr. B* 34 (1978) 64.

[30] T. Nilges, A. Pfitzner, *Z. Kristallogr.* 220 (2005) 281.